

**Outer membrane *c*-type cytochromes OmcA and MtrC play distinct roles in enhancing
the attachment of *Shewanella oneidensis* MR-1 cells to goethite during dissimilatory iron
reduction**

Xinxin Jing^{1,#}, Yichao Wu^{1,#}, Liang Shi^{2,3}, Caroline L. Peacock⁴, Noha Mohamed Ashry^{1,5},

Chunhui Gao¹, Qiaoyun Huang¹, Peng Cai^{*1}

1 State Key Laboratory of Agricultural Microbiology, College of Resources and Environment,

Huazhong Agricultural University, Wuhan, China

2 Department of Biological Sciences and Technology, School of Environmental Studies,

China University of Geosciences, Wuhan, China

3 State Key Laboratory of Biogeology and Environmental Geology, China University of

Geosciences, Wuhan, China

4 School of Earth and Environment, University of Leeds, Leeds LS2 9JT, UK

5 Agriculture Microbiology Department, Faculty of Agriculture, Benha University, Moshtohor,

Qalubia, 13736, Egypt

The authors contributed equally to this work. Author order was determined by level of contribution.

*Corresponding author: Peng Cai, cp@mail.hzau.edu.cn

Supplementary Methods:

Genotypic and phenotypic characterization. PCR amplification and immunolocalization were applied to characterize the genotypic and phenotypic traits of strains used in this study. *mtrC* was amplified with primer mtrC-F (5'-ACTGCCACGTTGATTCTGT-3') and mtrC-R (5'-ACATGCGTCAAGGCCTACAA-3'). *omcA* was amplified with primer omcA-F (5'-TGGAAAGCCCACGAAAGTGA-3') and omcA-R (5'-CTGCCTAAAGCGATAACCGT-3'). The antibodies against the hydrophilic and surface-exposed regions of MtrC and OmcA were produced as the previous study (1). The amino acid sequences of immunogenic peptides are GCKNGALDPKATIN (MtrC, 399-410) and GCHTEKPSAHHSSTD (OmcA, 349-364).

Iron oxides reduction assays. During the cell-mineral attachment experiment, QCM-D effluent was collected periodically in an acid-washed vial purged with nitrogen gas to prevent Fe(II) oxidized and precipitated. The Fe(II) concentration of QCM-D effluent were measured by the ferrozine assay (2) after extracted in 0.5 M HCl overnight. Fe(II) concentration were determined using ferrous ammonium sulfate as a standard solution.

Table S1. IR band assignments for *Shewanella*

| Wavenumber (cm ⁻¹) | IR band assignment |
|--------------------------------|--|
| 1742 | $\nu(C=O)$ in COOH of OmcA, MtrC(3) |
| 1729–1720 | C=O stretch in COOH(4, 5) |
| 1700-1600 | amide I: C=O stretching, -CN and –NH bending in amines(6) |
| 1550-1540 | amide II: N-H bending, C-N stretching(4-6) |
| 1482-1454 | bending of CH ₂ /CH ₃ (4, 5) |
| 1450-1360 | $\nu_s(COO^-)$ (4) |
| 1260-1220 | $\nu_{as}(PO_2^-)$ (5) |
| 1160-1150 | $\nu_s(P-O)$ of phosphoryl surface complexes(6) |
| 1120-1110 | $\nu(P=O)$ (6) |
| 1118-1114 | $\nu(C-O-P,P-O-P)$,ring vibrations(4, 5) |
| 1094-1080 | $\nu_s(PO_2^-)$; ring vibrations; $\nu(C-O)$; P=O stretch in phosphodiester, phosphorylated proteins, and polyphosphates(4, 6) |
| 1078-1048 | C–OH, C–O–C, and C–C vibrations of polysaccharides(4) |
| 1045 | $\nu(P-OFe)$ (6) |
| 1043-1039 | $\nu(P-OH,P-OFe)$ (4, 5) |
| 1020-1016 | $\nu(P-OFe)$, ring vibrations(4, 5) |
| 1011-995 | $\nu_{as}(P-(OFe)_2)$ (6) |
| 979-962 | symmetric stretching of PO ₃ and PO ₂ (4, 6) |
| 955-950 | $\nu(P-OH,P-OFe)$ (6) |
| 930-927 | $\nu_s(P-(OFe)_2)$ (6) |
| 886 | $\delta(OH)$ of goethite(6) |

Table S2. Signs of each cross-peak in the 2D correlation maps of WT cells during short-term attachment (Figure S7A, B). “0” indicates no cross peak in the position.

| | 1645 | 1543 | 1087 | 1053 | 1046 |
|------|------|------|------|-------|-------|
| 1645 | + | +(0) | +(+) | +(+) | +(+) |
| 1543 | | + | +(+) | +(+) | +(+) |
| 1087 | | | + | + (0) | + (0) |
| 1053 | | | | + | + (0) |
| 1046 | | | | | 0 |

peak intensity: $v_s(\text{PO}_2^-)(1087 \text{ cm}^{-1}) > v(\text{P-OFe})(1053 \text{ cm}^{-1}) > \text{amide II}(1543 \text{ cm}^{-1}) > \text{amide I}(1645 \text{ cm}^{-1})$

reaction sequences: $v_s(\text{PO}_2^-)(1087 \text{ cm}^{-1}), v(\text{C-OH/ C-O-C/C-C}) (1053 \text{ cm}^{-1}), v(\text{P-OFe}) (1046 \text{ cm}^{-1}) > \text{amide I}(1645 \text{ cm}^{-1}), \text{amide II}(1543 \text{ cm}^{-1})$

Table S3. Signs of each cross-peak in the 2D correlation maps of WT cells during long-term attachment (Figure S7C, D). “0” indicates no cross peak in the position.

| | 1645 | 1546 | 1398 | 1076 | 1048 |
|------|------|------|-------|-------|-------|
| 1645 | + | +(+) | +(0) | +(+) | 0(+) |
| 1546 | | + | + (0) | + (+) | 0 (+) |
| 1458 | | | + | + (+) | 0 (+) |
| 1398 | | | | + | 0 (0) |
| 1076 | | | | | 0 |

peak intensity: $\nu(\text{C}-\text{OH}/ \text{C}-\text{O}-\text{C}/\text{C}-\text{C}) (1076 \text{ cm}^{-1}) > \text{amide II}(1546 \text{ cm}^{-1}) > \text{amide I}(1645 \text{ cm}^{-1}) > \nu_s(\text{COO}^-)(1398 \text{ cm}^{-1})$

reaction sequences: $\nu(\text{C}-\text{OH}/ \text{C}-\text{O}-\text{C}/\text{C}-\text{C})(1076 \text{ cm}^{-1}) > \text{amide II}(1546 \text{ cm}^{-1}) > \text{amide I}(1645 \text{ cm}^{-1})$

Table S4. Signs of each cross-peak in the 2D correlation maps of $\Delta mtrC$ cells during short-term attachment (Figure 5A, B). “0” indicates no cross peak in the position.

| | 1648 | 1550 | 1238 | 1079 | 1040 |
|------|------|------|------|------|------|
| 1648 | + | +(+) | +(+) | +(+) | 0(0) |
| 1550 | | + | +(+) | +(+) | 0(0) |
| 1238 | | | + | +(+) | 0(+) |
| 1079 | | | | + | 0(0) |
| 1040 | | | | | 0 |

peak intensity: $v_s(\text{PO}_2^-)(1079 \text{ cm}^{-1}) > \text{amide I}(1648 \text{ cm}^{-1}) > \text{amide II}(1550 \text{ cm}^{-1}) > v_{as}(\text{PO}_2^-)(1238 \text{ cm}^{-1})$

reaction sequences: $v_s(\text{PO}_2^-)(1079 \text{ cm}^{-1}) > v_{as}(\text{PO}_2^-)(1238 \text{ cm}^{-1}) > \text{amide II}(1550 \text{ cm}^{-1}) > \text{amide I}(1648 \text{ cm}^{-1})$

Table S5. Signs of each cross-peak in the 2D correlation maps of $\Delta omcA$ - $\Delta mtrC$ cells during short-term attachment (Figure S8A, B). “0” indicates no cross peak in the position.

| | 1644 | 1548 | 1404 | 1236 | 1082 | 1051 | 1040 |
|------|------|-------|-------|-------|-------|-------|-------|
| 1644 | + | + (0) | + (+) | + (0) | + (+) | + (+) | 0 (+) |
| 1549 | | + | + (+) | + (0) | + (+) | + (+) | 0 (+) |
| 1404 | | | + | + (-) | + (+) | + (+) | 0 (+) |
| 1236 | | | | + | + (+) | + (+) | 0 (0) |
| 1082 | | | | | + | + (0) | 0 (+) |
| 1051 | | | | | | + | 0 (+) |
| 1040 | | | | | | | 0 |

peak intensity: $v_s(\text{PO}_2^-)(1082 \text{ cm}^{-1}) > v(\text{C}-\text{OH}/ \text{C}-\text{O}-\text{C/C-C})(1051 \text{ cm}^{-1}) >$ amide I(1644 cm^{-1}) $>$ amide II(1548 cm^{-1}) $>$ $v_s(\text{COO}^-)(1404 \text{ cm}^{-1}) > v_{\text{as}}(\text{PO}_2^-)(1236 \text{ cm}^{-1})$

reaction sequences: $v(\text{C}-\text{OH}/ \text{C}-\text{O}-\text{C/C-C})(1051 \text{ cm}^{-1}), v_s(\text{PO}_2^-)(1082 \text{ cm}^{-1}) > v_s(\text{COO}^-)(1404 \text{ cm}^{-1}) >$ amide I(1644 cm^{-1}) $>$ amide II(1548 cm^{-1}), $v_{\text{as}}(\text{PO}_2^-)(1236 \text{ cm}^{-1})$

Table S6. Signs of each cross-peak in the 2D correlation maps of $\Delta omcA$ cells during short-term attachment (Figure 6A, B). “0” indicates no cross peak in the position.

| | 1646 | 1548 | 1462 | 1400 | 1236 | 1086 | 1046 | 943 |
|------|------|------|------|------|------|------|------|------|
| 1646 | + | +(+) | +(+) | +(-) | +(0) | +(+) | +(+) | +(+) |
| 1548 | | + | +(+) | +(-) | +(-) | +0) | +(+) | +(+) |
| 1462 | | | + | +(-) | +(-) | +(-) | +(-) | 0(0) |
| 1400 | | | | + | +0) | +(+) | +(+) | 0(+) |
| 1236 | | | | | + | +(+) | +(+) | +(+) |
| 1086 | | | | | | + | +0) | +(+) |
| 1049 | | | | | | | 0 | +0) |
| 943 | | | | | | | | + |

peak intensity: amide I(1646 cm^{-1}) > amide II(1548 cm^{-1}) > $v_s(\text{PO}_2^-)$ (1086 cm^{-1})> $v(\text{P-OFe})$ (1046 cm^{-1})> $v_{as}(\text{PO}_2^-)$ (1236 cm^{-1}) > $v_s(\text{COO}^-)$ (1400 cm^{-1})> $\delta(\text{CH}_3/\text{CH}_2)$ (1462 cm^{-1}) > $v_s(\text{P-(OFe)}_2)$ (943 cm^{-1})

reaction sequences: $\delta(\text{CH}_3/\text{CH}_2)$ (1462 cm^{-1}) > $v(\text{P-OFe})$ (1046 cm^{-1}), $v_s(\text{PO}_2^-)$ (1086 cm^{-1}), amide II(1548 cm^{-1}) > amide I(1646 cm^{-1}) > $v_s(\text{COO}^-)$ (1400 cm^{-1})

Table S7. Signs of each cross-peak in the 2D correlation maps of $\Delta omcA$ cells during long-term attachment (Figure 6C, D). “0” indicates no cross peak in the position.

| | 1641 | 1548 | 1065 | 1044 |
|------|------|------|------|------|
| 1641 | + | +(-) | +(-) | 0(0) |
| 1548 | | + | +(-) | 0(0) |
| 1065 | | | + | 0(0) |
| | | | | 0 |

peak intensity: $\nu(\text{C}-\text{OH}/\text{C}-\text{O}-\text{C}/\text{C}-\text{C})(1065 \text{ cm}^{-1}) > \text{amide II}(1548 \text{ cm}^{-1}) > \text{amide I}(1641 \text{ cm}^{-1})$

reaction sequences: amide I(1641 cm^{-1}) > amideII (1548 cm^{-1}) > $\nu(\text{C}-\text{OH}/\text{C}-\text{O}-\text{C}/\text{C}-\text{C})(1065 \text{ cm}^{-1})$

Table S8. Signs of each cross-peak in the 2D correlation maps of $\Delta mtrC$ cells during long-term attachment (Figure 5C, D). “0” indicates no cross peak in the position.

| | 1648 | 1550 | 1397 | 1226 | 1085 | 1040 |
|------|------|------|------|------|------|------|
| 1648 | + | +(+) | +(-) | +(-) | +(-) | 0(-) |
| 1550 | | + | +(-) | +(-) | +(-) | 0(-) |
| 1397 | | | + | +(-) | +(-) | 0(0) |
| 1226 | | | | + | +(+) | 0(-) |
| 1085 | | | | | + | 0 |

peak intensity: $v_s(\text{PO}_2^-)(1085 \text{ cm}^{-1}) > \text{amide I}(1648 \text{ cm}^{-1}) > \text{amide II}(1550 \text{ cm}^{-1}) > v_{as}(\text{PO}_2^-)(1226 \text{ cm}^{-1}) > v_s(\text{COO}^-)(1397 \text{ cm}^{-1})$

reaction sequences: amide II(1550 cm⁻¹)> amide I(1648 cm⁻¹)> $v_s(\text{PO}_2^-)(1085 \text{ cm}^{-1}) > v_s(\text{COO}^-)(1397 \text{ cm}^{-1}) > v_{as}(\text{PO}_2^-)(1226 \text{ cm}^{-1})$

Table S9. Signs of each cross-peak in the 2D correlation maps of $\Delta omcA$ - $\Delta mtrC$ cells during long-term attachment (Figure S8C, D). “0” indicates no cross peak in the position.

| | 1648 | 1551 | 1224 | 1084 | 1059 | 1049 |
|------|------|------|------|------|------|------|
| 1648 | + | +(+) | +(-) | +(-) | +(-) | 0(0) |
| 1551 | | + | +(-) | +(-) | +(-) | 0(0) |
| 1224 | | | + | +(+) | +(+) | 0(0) |
| 1084 | | | | + | +(-) | 0(-) |
| 1059 | | | | | + | 0(0) |
| 1049 | | | | | | 0 |

peak intensity: $v_s(\text{PO}_2^-)(1084 \text{ cm}^{-1}) > v(\text{C-OH/ C-O-C/C-C})(1059 \text{ cm}^{-1}) > \text{amide I}(1648 \text{ cm}^{-1}) > \text{amide II}(1551 \text{ cm}^{-1}) > v_{as}(\text{PO}_2^-)(1224 \text{ cm}^{-1})$

reaction sequences: $\text{amide II}(1551 \text{ cm}^{-1}) > \text{amide I}(1648 \text{ cm}^{-1}) > v_s(\text{PO}_2^-)(1084 \text{ cm}^{-1}) > v(\text{C-OH/ C-O-C/C-C})(1059 \text{ cm}^{-1}) > v_{as}(\text{PO}_2^-)(1224 \text{ cm}^{-1})$

Table S10. The adhesion forces and rupture length of four strains in AFM analysis. Different letters following the mean values \pm SE (n=100) indicate significant differences among the strains ($P<0.05$).

| | Adhesion forces (nN) | Rupture length (nm) |
|---------------------------|----------------------|----------------------|
| WT | 1.17 \pm 0.05 a | 292.33 \pm 11.35 a |
| $\Delta mtrC$ | 1.18 \pm 0.05 a | 182.64 \pm 6.94 b |
| $\Delta omcA$ | 0.71 \pm 0.03 b | 99.02 \pm 4.80 d |
| $\Delta omcA-\Delta mtrC$ | 0.75 \pm 0.03 b | 132.02 \pm 7.43 c |

Table S11. Fe(II) concentration of QCM-D effluent during the cell-mineral attachment experiment

| Strain | Fe(II) concentration ($\mu\text{g}/\text{ml}$) | | | | | | |
|-----------------------------|--|-------------------|-------------------|-------------------|-------------------|-------------------|-------------------|
| | 0 h | 0.5 h | 1 h | 3 h | 5 h | 8 h | 11 h |
| Abiotic control | 0.043 \pm 0.005 | 0.050 \pm 0.010 | 0.035 \pm 0.005 | 0.046 \pm 0.013 | 0.047 \pm 0.038 | 0.054 \pm 0.003 | 0.041 \pm 0.005 |
| WT | 0.030 \pm 0.008 | 0.045 \pm 0.004 | 0.052 \pm 0.008 | 0.041 \pm 0.001 | 0.041 \pm 0.001 | 0.050 \pm 0.005 | 0.049 \pm 0.006 |
| $\Delta omcA$ | 0.036 \pm 0.005 | 0.042 \pm 0.002 | 0.041 \pm 0.004 | 0.047 \pm 0.005 | 0.046 \pm 0.005 | 0.053 \pm 0.004 | 0.051 \pm 0.003 |
| $\Delta mtrC$ | 0.068 \pm 0.006 | 0.045 \pm 0.001 | 0.043 \pm 0.006 | 0.051 \pm 0.005 | 0.044 \pm 0.002 | 0.044 \pm 0.009 | 0.048 \pm 0.005 |
| $\Delta omcA - \Delta mtrC$ | 0.032 \pm 0.001 | 0.059 \pm 0.002 | 0.040 \pm 0.000 | 0.040 \pm 0.001 | 0.036 \pm 0.001 | 0.037 \pm 0.001 | 0.039 \pm 0.001 |

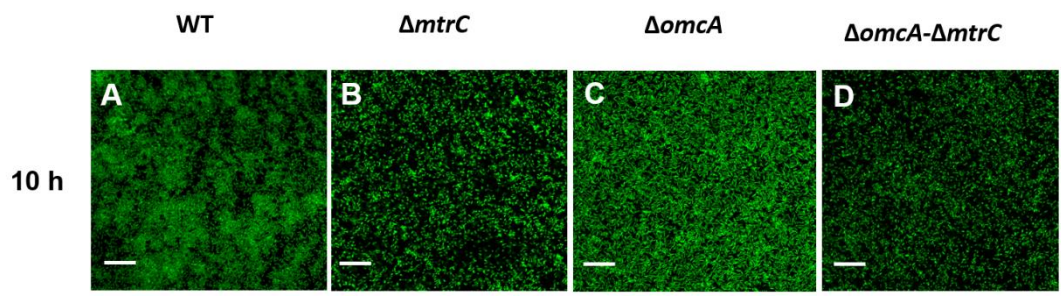


Fig. S1. The microscopic images of QCM-D sensors after 10-h attachment, the bar is 20 μm .

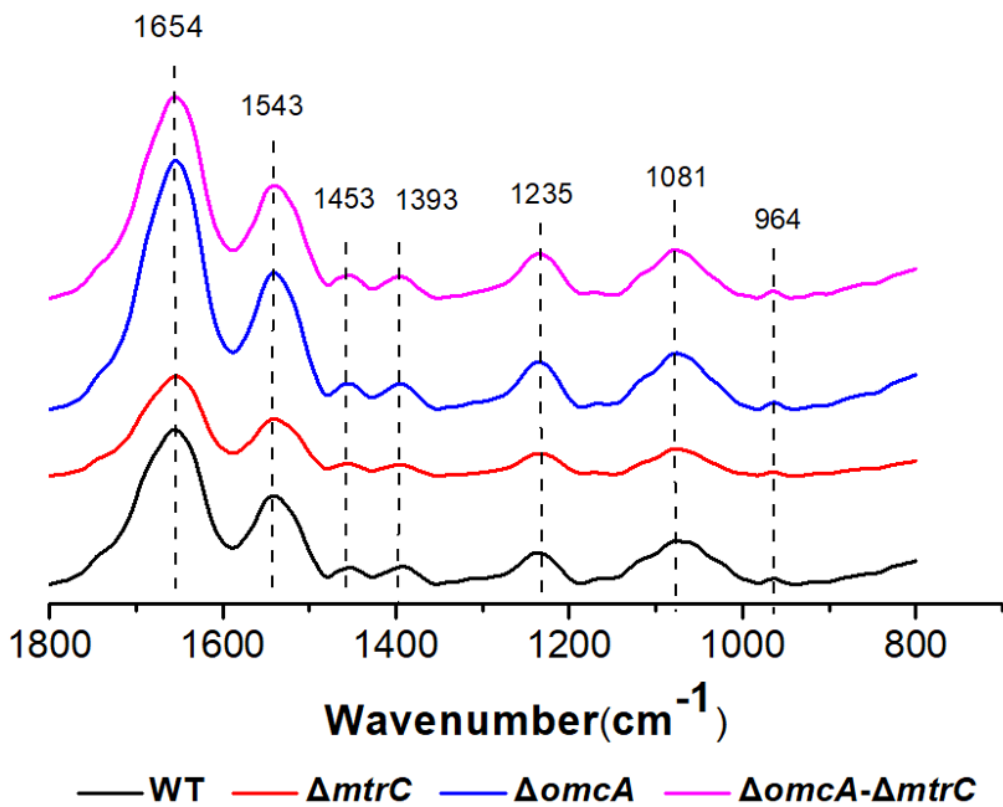


Fig. S2. ATR-FTIR spectra of goethite-free *Shewanella* cells.

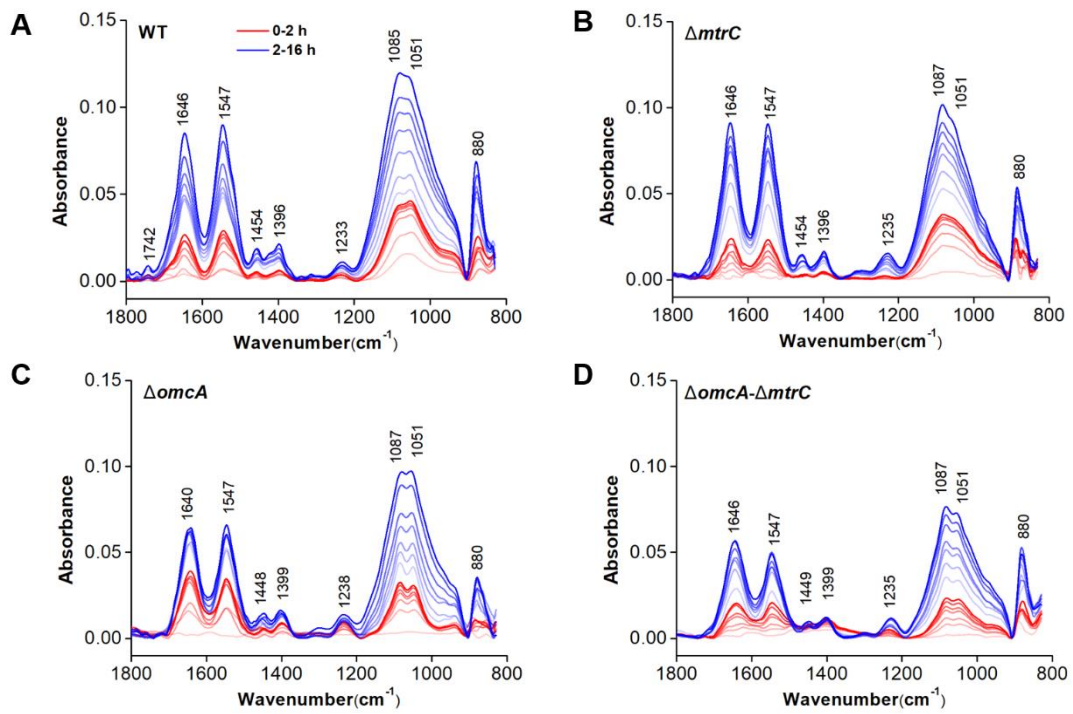


Fig. S3. ATR-FTIR spectra of WT (A), $\Delta mtrC$ (B), $\Delta omcA$ (C) and $\Delta omcA-\Delta mtrC$ (D)

attachment to goethite during short-term (0-2 h) and long-term (2-16 h).

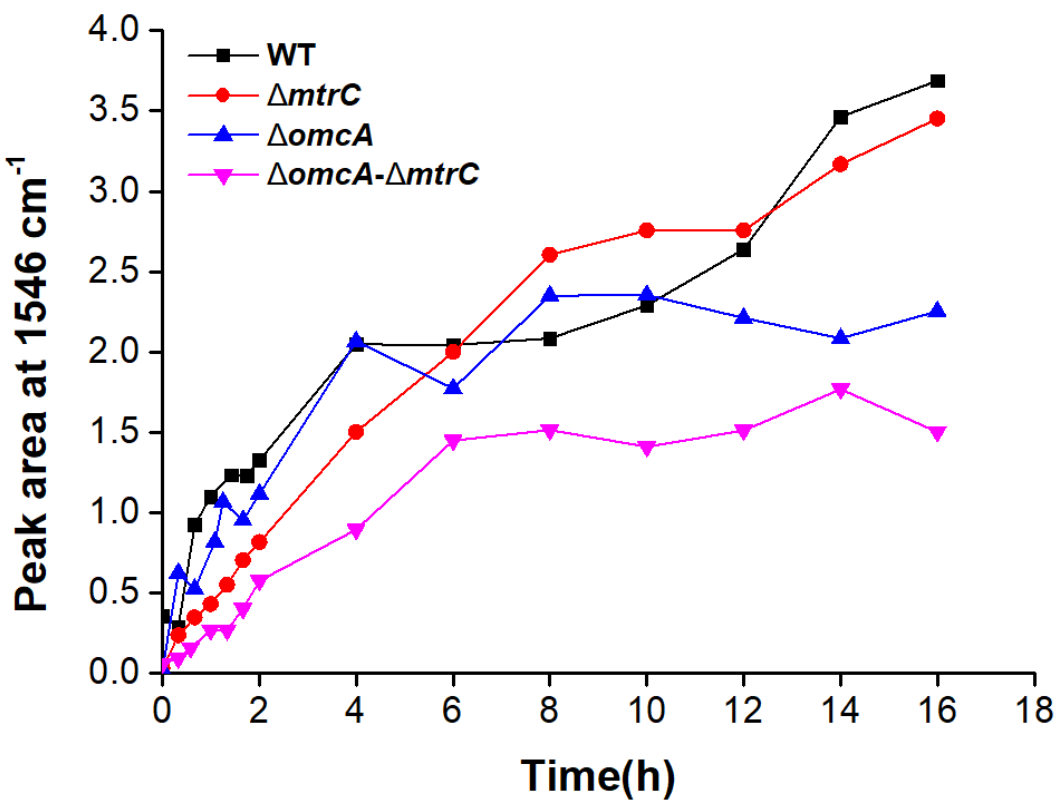


Fig. S4. The changes of peak area for amide II (1543 cm^{-1}) as a function of time.

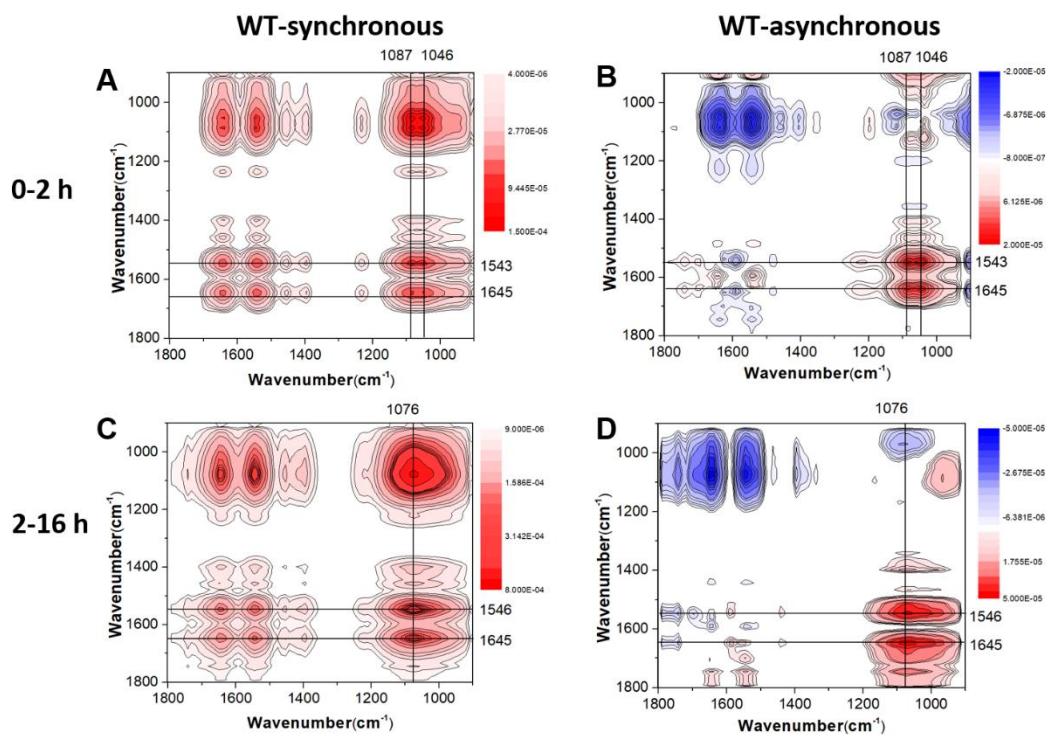


Fig. S5. Synchronous (A, C) and asynchronous (B, D) 2D correlation map of time-dependent ATR-FTIR spectra for the short-term (A, B) and long-term (C, D) attachment of WT cells to goethite. The red and blue regions represent positive and negative correlations intensities.

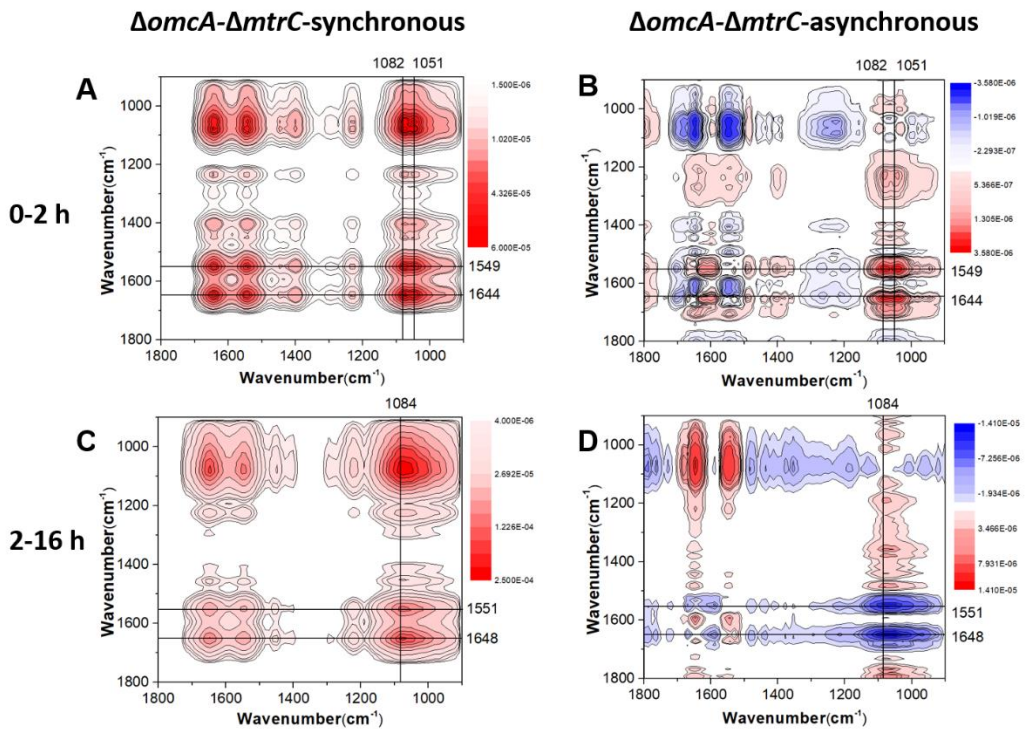


Fig. S6. Synchronous (A, C) and asynchronous (B, D) 2D correlation map of time-dependent ATR-FTIR spectra for the short-term (A, B) and long-term (C, D) attachment of $\Delta omcA\text{-}\Delta mtrC$ cells to goethite. The red and blue regions represent positive and negative correlations intensities.

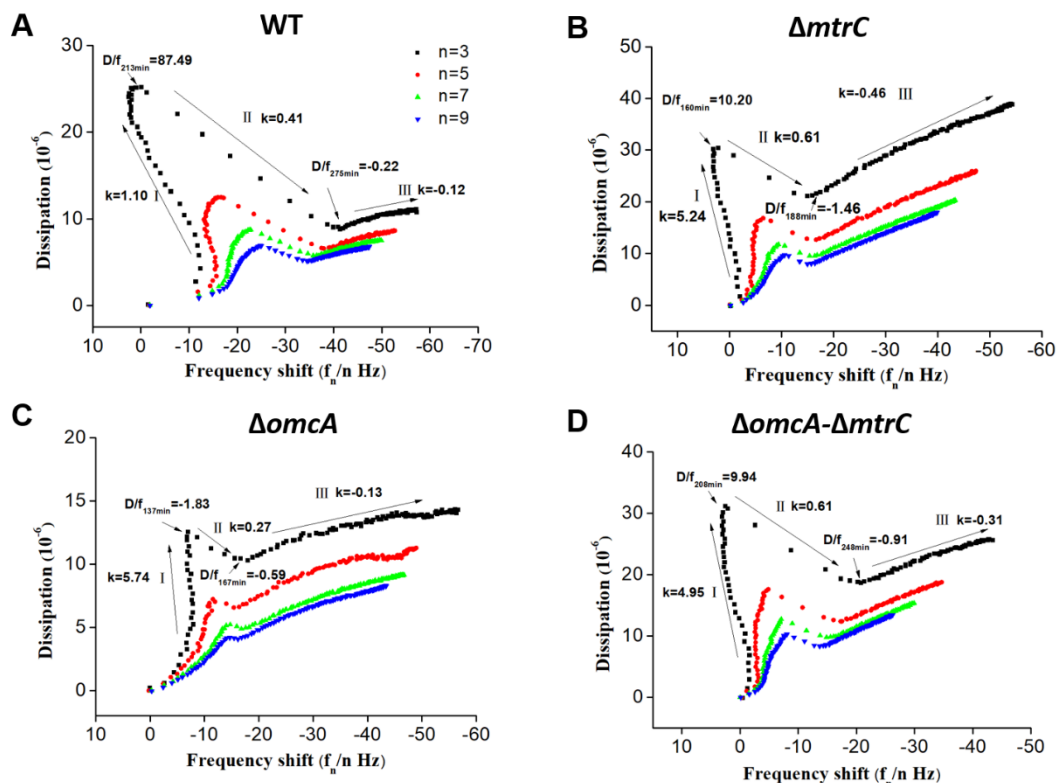


Fig. S7. QCM-D $\Delta D-\Delta f$ plots for *Shewanella* cells attached on goethite surface.

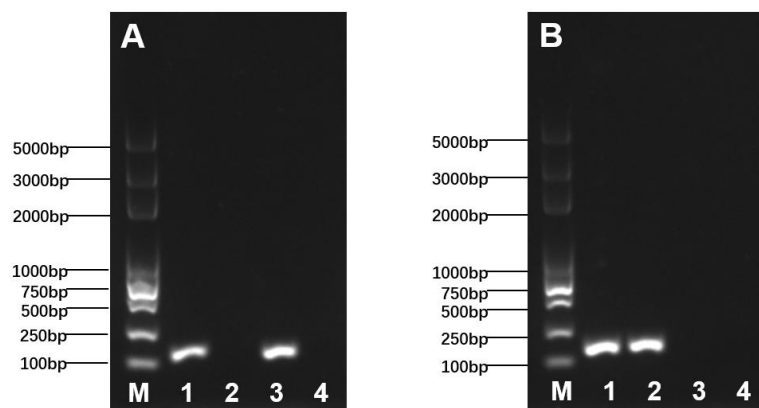


Fig. S8. Validation of PCR products by gel electrophoresis. M: DL5000 marker; Lane 1-4: Amplification frag-ment of the *S. oneidensis* MR-1 WT (1), Δ omcA (2), Δ mtrC (3), Δ omcA- Δ mtrC (4) using primer pairs of omcA-F and omcA-R(A), mtrC-F and mtrC-F(B).

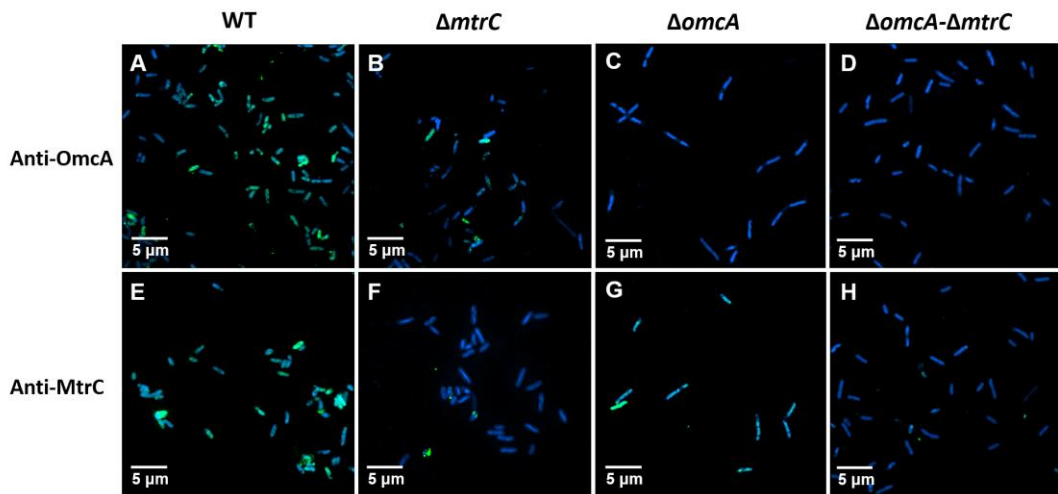


Fig. S9. Structured illumination microscopy images of WT (A, E), $\Delta mtrC$ (B, F), $\Delta omcA$ (C, G) and $\Delta omcA\text{-}\Delta mtrC$ (D, H) stained by DAPI (blue). Outer membrane OmcA and MtrC were specific labeled with antibodies against OmcA (A-D, green) or MtrC (E-H, green).

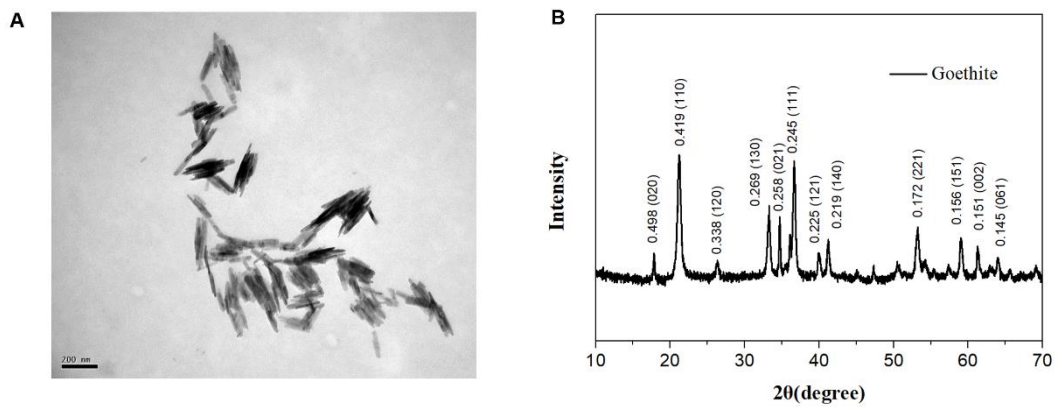


Fig. S10. Transmission electron microscopic (TEM) images of goethite (A). Powder X-ray diffraction (XRD) patterns of goethite (B).

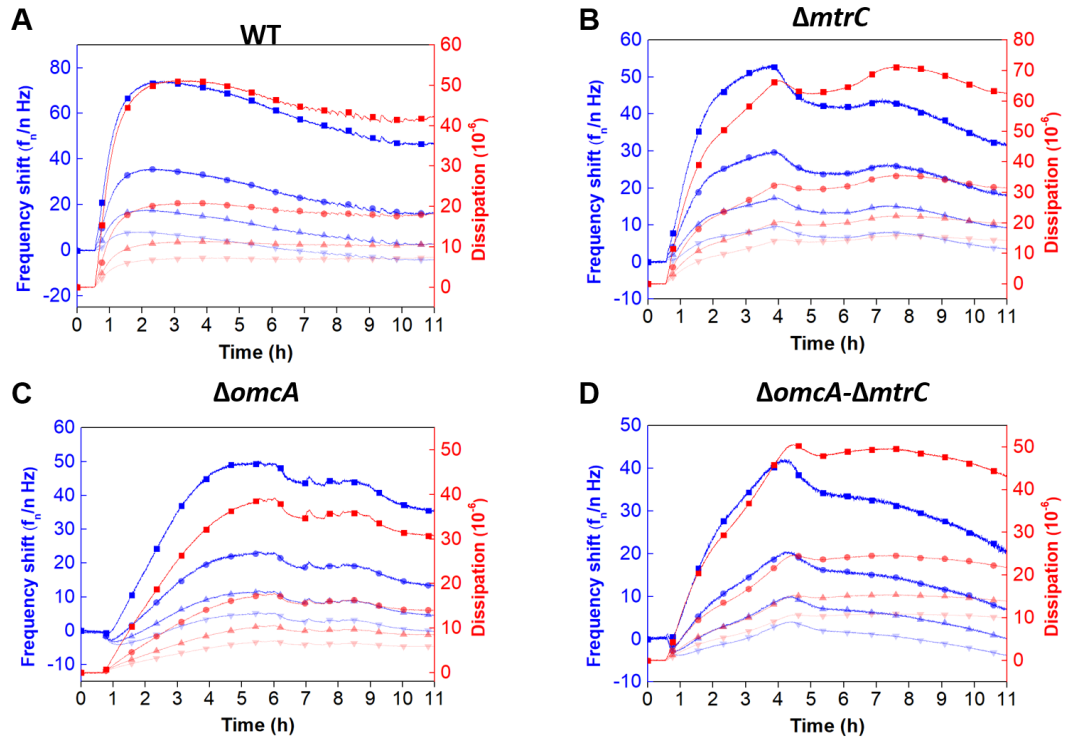


Fig. S11. The frequency (Δf) and dissipation (ΔD) shift for the attachment of WT (A), $\Delta mtrC$ (B), $\Delta omcA$ (C) and $\Delta omcA-\Delta mtrC$ (D) on golden sensors.

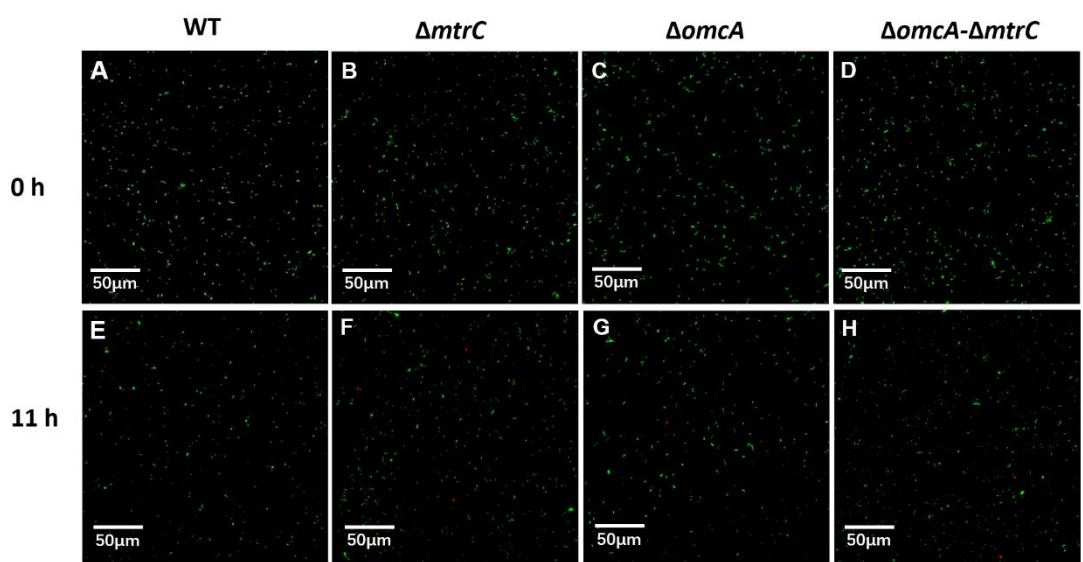


Fig. S12. Fluorescence microscopic images of WT (A, E), $\Delta mtrC$ (B, F), $\Delta omcA$ (C, G) and $\Delta omcA-\Delta mtrC$ (D, H) incubated in 0.1 M NaCl for 0 hours and 11 hours.

Reference

1. Marshall MJ, Beliaev AS, Dohnalkova AC, Kennedy DW, Shi L, Wang Z, Boyanov MI, Lai B, Kemner KM, McLean JS, Reed SB, Culley DE, Bailey VL, Simonson CJ, Saffarini DA, Romine MF, Zachara JM, Fredrickson JK. 2006. *c*-Type Cytochrome-Dependent Formation of U(IV) Nanoparticles by *Shewanella oneidensis*. PLOS Biology 4:e268.
2. Stookey LL. 1970. Ferrozine - a new spectrophotometric reagent for iron. Analytical Chemistry 42:779-781.
3. You LX, Rao L, Tian XC, Wu RR, Wu X, Zhao F, Jiang YX, Sun SG. 2015. Electrochemical in situ FTIR spectroscopy studies directly extracellular electron transfer of *Shewanella oneidensis* MR-1. Electrochim Acta 170:131-139.
4. Elzinga EJ, Huang JH, Chorover J, Kretzschmar R. 2012. ATR-FTIR spectroscopy study of the influence of pH and contact time on the adhesion of *Shewanella putrefaciens* bacterial cells to the surface of hematite. Environ Sci Technol 46:12848-12855.
5. Parikh SJ, Chorover J. 2006. ATR-FTIR Spectroscopy Reveals Bond Formation During Bacterial Adhesion to Iron Oxide. Langmuir 22:8492-8500.
6. Yan W, Wang H, Jing C. 2016. Adhesion of *Shewanella oneidensis* MR-1 to Goethite: A Two-Dimensional Correlation Spectroscopic Study. Environ Sci Technol 50:4343-4349.